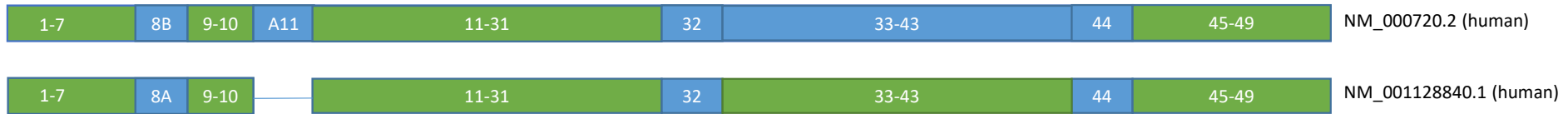
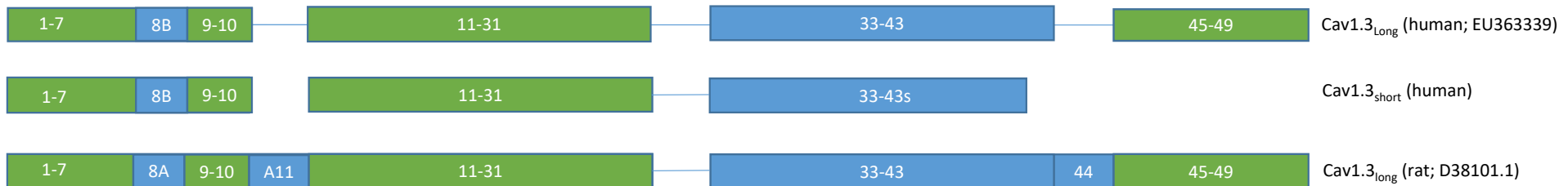


## Figure S1

**a**



**b**



**Figure S1.** Schematic drawing of the human and rat *CACNA1D* isoforms used. (a) Isoforms used as reference sequence for sequence analysis of *CACNA1D* in SND patients (NM\_000720.2 and NM\_001128840.1) and (b) used as template cDNA for cloning of mutant and wild-type expression constructs (EU363339= Cav1.3<sub>Long</sub>, D38101.1=rat Cav1.3<sub>Long</sub>). Exons present in all isoforms are indicated in green. The short Cav1.3  $\alpha_1$  isoform used for functional analysis uses an alternative splice site in exon 43 encoding a C-terminally truncated Cav1.3 protein.

## Figure S2

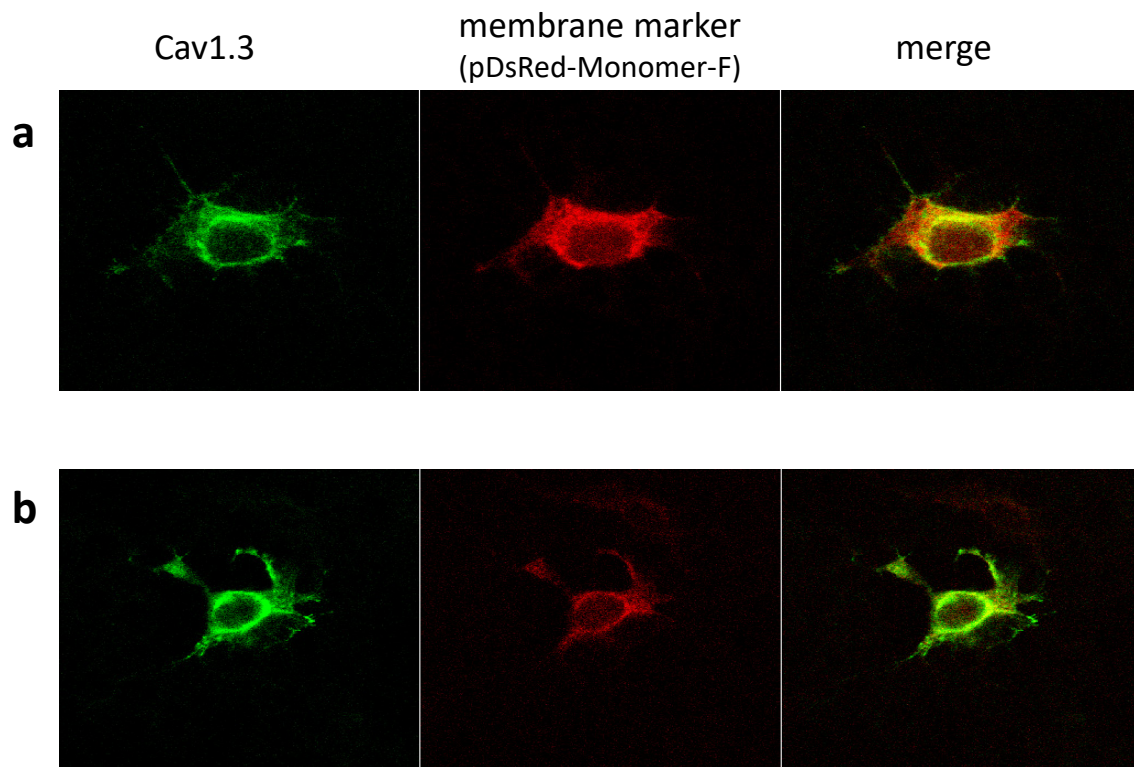


**Figure S2.** Cellular localization of mutant Cav1.3<sub>L</sub> R930H. **(a)** HEK293T cells were transiently transfected with WT and **(b)** mutant Cav1.3 and the accessory subunits Cav  $\beta_2$  and Cav  $\alpha_2\delta_1$ . Cav1.3<sub>L</sub> proteins are labeled in green and the co-transfected membrane marker (pDsRed-Monomer-F) is labeled in red.

## Figure S3

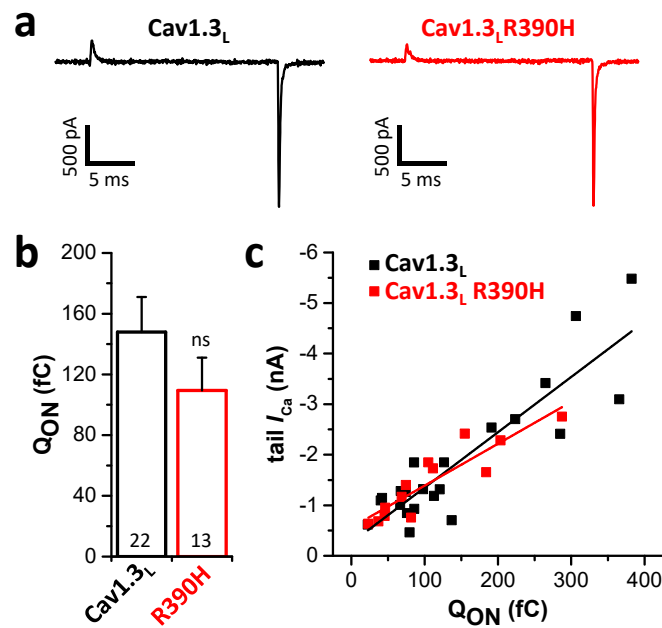


**Figure S3.** Coupling of ON-gating current to the opening of Cav<sub>L</sub> and Cav<sub>L</sub>R390H. (a) ON-gating currents were measured stepping from a holding potential of -80 mV to the reversal potential of each cell. Tail currents were induced by a repolarisation step to -80 mV. Illustrated are representative Q<sub>ON</sub> and tail current traces for Cav1.3<sub>L</sub> (black) and Cav1.3<sub>L</sub> R390H (red). (b) Quantification of the integral of the ON-gating current for Cav1.3<sub>L</sub> and Cav1.3<sub>L</sub>R390H revealed a non-significant reduction of Q<sub>ON</sub> for R930H. Numbers of cells analyzed are illustrated within the bar graph. Data are provided as mean ± S.E.M.. (c) Correlation of Q<sub>ON</sub> and the peak tail current amplitude (tail I<sub>Ca</sub>).

## Figure S4

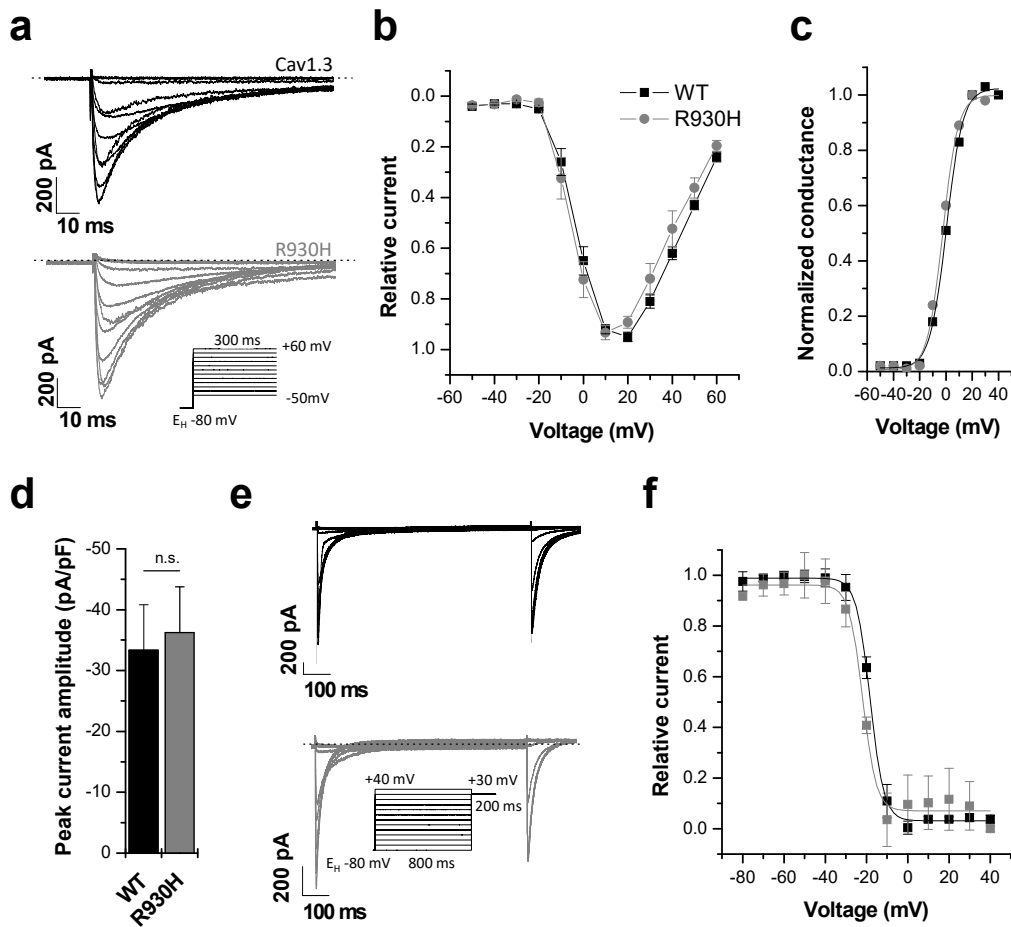


**Figure S4.** Functional characterization of the rCav1.3<sub>L</sub> R930H mutation of the rat Cav1.3 channel. (a) Whole-cell patch clamp recordings of wild-type rCav1.3<sub>L</sub> and the respective mutant rCav1.3<sub>L</sub> R930H channel transiently transfected in CHO cells. Representative current traces of wild-type rCav1.3<sub>L</sub> and the respective mutant rCav1.3<sub>L</sub> R930H. (b) Illustration of the current-voltage relationship and (c) the conductance-voltage relationships of wild-type rCav1.3<sub>L</sub> and mutant rCav1.3<sub>L</sub> R930H. (d) Analysis of the peak current densities of the wild-type rCav1.3<sub>L</sub> and mutant rCav1.3<sub>L</sub> R930H. (e) Representative current traces of voltage-dependence of inactivation recordings for wild-type rCav1.3<sub>L</sub> and mutant rCav1.3<sub>L</sub> R930H and (f) the corresponding analysis of the voltage-dependence of inactivation. Data are presented as mean  $\pm$  S.E.M.

## Figure S5

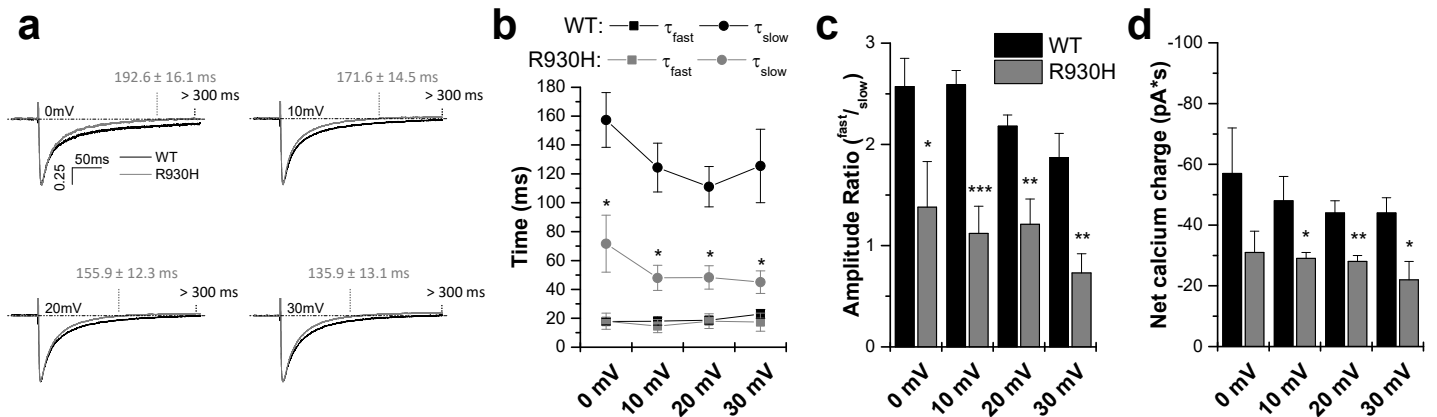


**Figure S5.** *R930H causes an enhanced inactivation in a long transcript variant of the rat Cav1.3 channel (rCav1.3<sub>L</sub>).* (a) Analysis of the inactivation kinetics of wild-type rCav1.3<sub>L</sub> and mutant rCav1.3<sub>L</sub> R930H. Illustration of the time necessary to reach full inactivation for wild-type rCav1.3<sub>L</sub> and mutant rCav1.3<sub>L</sub> R930H. (b) Fast and slow time constants of inactivation for wild-type rCav1.3<sub>L</sub> and mutant rCav1.3<sub>L</sub> R930H, illustrating an enhanced speed of the slow time constant of inactivation for the rCav1.3<sub>L</sub> R930H.  $\tau_1$  = fast component or time constant of inactivation.  $\tau_2$  = slow component or time constant of inactivation. (c) Ratio of the amplitudes for the fast and slow components of inactivation, analyzed for wild-type rCav1.3<sub>L</sub> and mutant rCav1.3<sub>L</sub> R930H. The data indicates a reduced contribution of the fast component of inactivation. (d) Net Ca<sup>2+</sup> flux of wild-type rCav1.3<sub>L</sub> and mutant rCav1.3<sub>L</sub> R930H, analyzed by the integral of the currents recorded at different potentials. The reduced integrals (in pA\*s) indicate a significant loss-of-function caused by the mutant rCav1.3<sub>L</sub> R930H. Data are shown as mean ± S.E.M.

## Figure S6

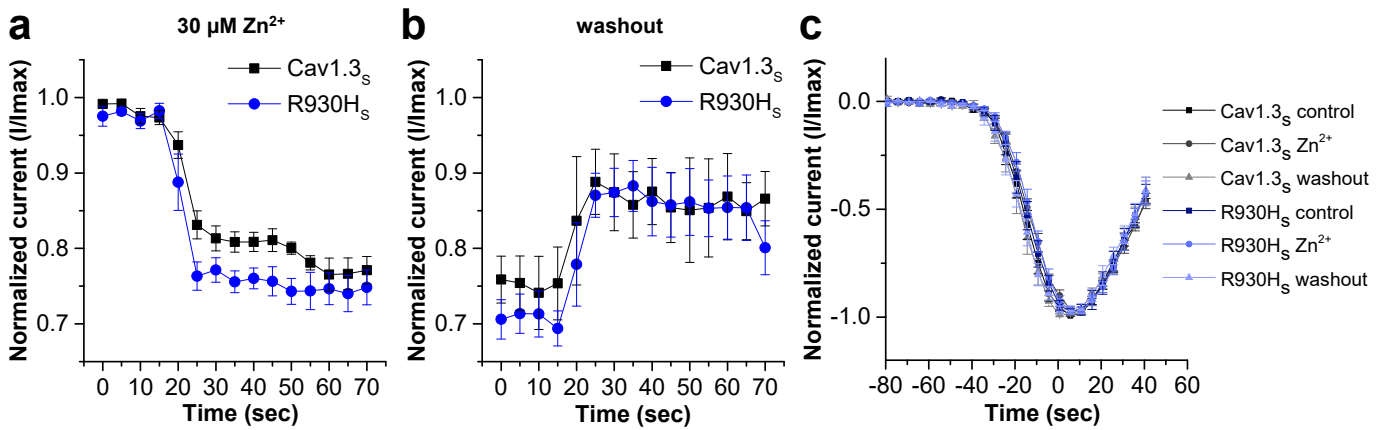


**Figure S6.** Inhibition of  $I_{Ca}$  from Cav1.3<sub>S</sub> and R930H<sub>S</sub> subunits by  $Zn^{2+}$ . (a) Effect of application of 30  $\mu M$   $Zn^{2+}$  on  $I_{Ca}$  mediated by Cav1.3<sub>S</sub> or R930H<sub>S</sub> upon depolarization to  $V_{max}$  at 0.2 Hz. In both mutant and wild-type channels, 30  $\mu M$   $Zn^{2+}$  significantly inhibited  $I_{Ca}$  (fraction of remaining current before  $Zn^{2+}$  application: Cav1.3<sub>S</sub>:  $0.99 \pm 0.01$ , R930H<sub>S</sub>:  $1.01 \pm 0.01$  and after application Cav1.3<sub>S</sub>:  $0.79 \pm 0.02$ ;  $p = 0.0002$ , R930H<sub>S</sub>:  $0.77 \pm 0.01$ ,  $p = 0.0009$ . Statistical analysis was performed with paired Student's t-test. (b)  $I_{Ca}$  inhibition by  $Zn^{2+}$  was reversible upon washout with standard bath solution (see Methods). Data are shown as mean  $\pm$  S.E.M.,  $n = 5$  for both constructs. (c) Normalized current-voltage relationships from Cav1.3<sub>S</sub> and R930H<sub>S</sub> before ( $n = 6$  for both), upon  $Zn^{2+}$  application ( $n = 6$  for both) and after washout ( $n = 5$  for both). Data are shown as mean  $\pm$  S.E.M..

**Table S1.** *Statistics of quality, mapping, coverage, depth and variant detection in each sample*

Sample ID	III_1	III_4	II_2	I_2
<b>Affection status</b>	affected	affected	affected	affected
<b>Total reads</b>	48,780,478	60,797,674	51,719,766	52,835,940
<b>Q30 [%]</b>	91.3	91.64	91.5	91.55
<b>Properly mapped reads [%]</b>	98.45	98.29	98.64	98.2
<b>Effective yield on target [Mb]</b>	4462.06	5688.75	4735.42	4666.76
<b>Average sequence depth on target [%]</b>	73.81	94.10	78.33	77.19
<b>Fraction of target that was covered with at least 20x [%]</b>	91.8	95.0	90.8	92.4
<b>Total variants</b>	306,483	359,244	323,320	352,639
SNP	265,171 (86,5%)	310,574 (86,5%)	279,503 (86,4%)	305,349 (86,6%)
InDel	41,312 (13,5%)	48,670 (13,5%)	43,817 (13,6%)	47,290 (13,4%)
<b>Variants total in CDS</b>	23,207	23,374	22918	22741
CDS SNP	22,499 (96,8%)	22,652 (96,8%)	22218 (96,9%)	22011 (96,8%)
CDS InDel	708 (3,2%)	722 (3,1%)	700 (3,1%)	731 (3,2%)
<b>Splice region variants total</b>	131	130	139	142
SNP	60 (46,2%)	59 (45,4%)	64 (46,0%)	62 (43,7%)
InDel	71 (53,8%)	71 (54,6%)	75 (54,0%)	80 (56,3%)

**Table S2.** List of shared variants and genes after WES of 4 affected family members

Gene	Disease*	Variant [c.]	Variant [p.]	MAF [%]	VarCards <sup>†</sup> [deleterious /all]	Gene Expression RPKM <sup>‡</sup> [heart]
SSX2IP	-	116T>C (NM_014021.3)	Leu39Pro	0.01	14/23	2.4
RNF207	Long QT syndrome	995delC (NM_207396.2)	Pro332LeufsTer44	-	-	5.9
RAB17	-	172A>G (NM_022449.3)	Lys58Glu	0.004	13/23	0.4
<b>CACNA1D</b>	<b>SANND, epilepsy, autism spectrum disorder, hyperaldosteronism</b>	<b>2789G&gt;A (NM_000720.3)</b>	<b>Arg930His</b>	<b>0.05</b>	<b>21/23</b>	<b>0.2</b>
MYH15	-	1417G>A (NM_014981.1)	Asp473Asn	0.0057	20/22	0.2
OSBPL11	-	511C>T (NM_022776.4)	Arg171Trp	0.0049	17/23	2.8
SCAP	Myocardial infarction	1427G>A (NM_012235.2)	Arg476Gln	0.01	14/23	4.8
ABCA8	Low HDL cholesterol	3262C>T (NM_007168.2)	Arg1088Cys	0.00024	13/23	10
BPTF	Developmental delay/intellectual disability & speech delay	5237A>G (NM_182641.3)	Asn1746Ser	0.00004	12/22	3
HDHD2	-	677G>A (NM_032124.4)	Gly226Glu	-	18/22	5
MED16	-	-18-1G>A (NM_005481.2)	?	-	-	2.8
TCF3	Hypogammaglobulinaemia and acute lymphoblastic leukaemia	1313G>A (NM_003200.3)	Arg438Gln	0.0049	14/23	1.6
IDH3G	-	167C>T(NM_004135.3)	Thr56Met	0.0016	14/21	18.4
MECP2	Rett syndrome	851C>T (NM_001110792.1)	MECP2	0.0007	19/21	4.2

\*associated disease in HGMD or ClinGen; <sup>†</sup>ratio of damaging/deleterious prediction in *in silico* algorithm; <sup>‡</sup> according to HPA RNA-seq normal tissue database; SANDD, sinoatrial node dysfunction and deafness; RPKM, reads per kilo base per million mapped reads